

Measurement of the CP -even fraction of $D^0 \rightarrow \pi^+ \pi^- \pi^+ \pi^-$

M. Ablikim¹, M. N. Achasov^{11,b}, P. Adlarson⁷⁰, M. Albrecht⁴, R. Aliberti³¹, A. Amoroso^{69A,69C}, M. R. An³⁵, Q. An^{66,53}, X. H. Bai⁶¹, Y. Bai⁵², O. Bakina³², R. Baldini Ferroli^{26A}, I. Balossino^{27A}, Y. Ban^{42,g}, V. Batzskaya^{1,40}, D. Becker³¹, K. Begzsuren²⁹, N. Berger³¹, M. Bertani^{26A}, D. Bettoni^{27A}, F. Bianchi^{69A,69C}, J. Bloms⁶³, A. Bortone^{69A,69C}, I. Boyko³², R. A. Briere⁵, A. Brueggemann⁶³, H. Cai⁷¹, X. Cai^{1,53}, A. Calcaterra^{26A}, G. F. Cao^{1,58}, N. Cao^{1,58}, S. A. Cetin^{57A}, J. F. Chang^{1,53}, W. L. Chang^{1,58}, G. Chelkov^{32,a}, C. Chen³⁹, Chao Chen⁵⁰, G. Chen¹, H. S. Chen^{1,58}, M. L. Chen^{1,53}, S. J. Chen³⁸, S. M. Chen⁵⁶, T. Chen¹, X. R. Chen^{28,58}, X. T. Chen¹, Y. B. Chen^{1,53}, Z. J. Chen^{23,h}, W. S. Cheng^{69C}, S. K. Choi⁵⁰, X. Chu³⁹, G. Cibinetto^{27A}, F. Cossio^{69C}, J. J. Cui⁴⁵, H. L. Dai^{1,53}, J. P. Dai⁷³, A. Dbeysi¹⁷, R. E. de Boer⁴, D. Dedovich³², Z. Y. Deng¹, A. Denig³¹, I. Denysenko³², M. Destefanis^{69A,69C}, F. De Mori^{69A,69C}, Y. Ding³⁶, J. Dong^{1,53}, L. Y. Dong^{1,58}, M. Y. Dong^{1,53,58}, X. Dong⁷¹, S. X. Du⁷⁵, P. Egorov^{32,a}, Y. L. Fan⁷¹, J. Fang^{1,53}, S. S. Fang^{1,58}, W. X. Fang¹, Y. Fang¹, R. Farinelli^{27A}, L. Fava^{69B,69C}, F. Feldbauer⁴, G. Felici^{26A}, C. Q. Feng^{66,53}, J. H. Feng⁵⁴, K. Fischer⁶⁴, M. Fritsch⁴, C. Fritsch⁶³, C. D. Fu¹, H. Gao⁵⁸, Y. N. Gao^{42,g}, Yang Gao^{66,53}, S. Garbolino^{69C}, I. Garzia^{27A,27B}, P. T. Ge⁷¹, Z. W. Ge³⁸, C. Geng⁵⁴, E. M. Gersabeck⁶², A. Gilman⁶⁴, K. Goetzen¹², L. Gong³⁶, W. X. Gong^{1,53}, W. Gradl³¹, M. Greco^{69A,69C}, L. M. Gu³⁸, M. H. Gu^{1,53}, Y. T. Gu¹⁴, C. Y. Guan^{1,58}, A. Q. Guo^{28,58}, L. B. Guo³⁷, R. P. Guo⁴⁴, Y. P. Guo^{10,f}, A. Guskov^{32,a}, T. T. Han⁴⁵, W. Y. Han³⁵, X. Q. Hao¹⁸, F. A. Harris⁶⁰, K. K. He⁵⁰, K. L. He^{1,58}, F. H. Heinsius⁴, C. H. Heinz³¹, Y. K. Heng^{1,53,58}, C. Herold⁵⁵, M. Himmelreich^{31,d}, G. Y. Hou^{1,58}, Y. R. Hou⁵⁸, Z. L. Hou¹, H. M. Hu^{1,58}, J. F. Hu^{51,i}, T. Hu^{1,53,58}, Y. Hu¹, G. S. Huang^{66,53}, K. X. Huang⁵⁴, L. Q. Huang^{28,58}, X. T. Huang⁴⁵, Y. P. Huang¹, Z. Huang^{42,g}, T. Hussain⁶⁸, N. Hüsken^{25,31}, W. Imoehl²⁵, M. Irshad^{66,53}, J. Jackson²⁵, S. Jaeger⁴, S. Janchiv²⁹, E. Jang⁵⁰, J. H. Jeong⁵⁰, Q. Ji¹, Q. P. Ji¹⁸, X. B. Ji^{1,58}, X. L. Ji^{1,53}, Y. Y. Ji⁴⁵, Z. K. Jia^{66,53}, H. B. Jiang⁴⁵, S. S. Jiang³⁵, X. S. Jiang^{1,53,58}, Y. Jiang⁵⁸, J. B. Jiao⁴⁵, Z. Jiao²¹, S. Jin³⁸, Y. Jin⁶¹, M. Q. Jing^{1,58}, T. Johansson⁷⁰, N. Kalantar-Nayestanaki⁵⁹, X. S. Kang³⁶, R. Kappert⁵⁹, B. C. Ke⁷⁵, I. K. Keshk⁴, A. Khoukaz⁶³, R. Kiuchi¹, R. Kliemt¹², L. Koch³³, O. B. Kolcu^{57A}, B. Kopf⁴, M. Kuemmel⁴, M. Kuessner⁴, A. Kupsc^{40,70}, W. Kühn³³, J. J. Lane⁶², J. S. Lange³³, P. Larin¹⁷, A. Lavania²⁴, L. Lavezzi^{69A,69C}, Z. H. Lei^{66,53}, H. Leithoff³¹, M. Lellmann³¹, T. Lenz³¹, C. Li⁴³, C. Li³⁹, C. H. Li³⁵, Cheng Li^{66,53}, D. M. Li⁷⁵, F. Li^{1,53}, G. Li¹, H. Li⁴⁷, H. Li^{66,53}, H. B. Li^{1,58}, H. J. Li¹⁸, H. N. Li^{51,i}, J. Q. Li⁴, J. S. Li⁵⁴, J. W. Li⁴⁵, Ke Li¹, L. J. Li¹, L. K. Li¹, Lei Li³, M. H. Li³⁹, P. R. Li^{34,j,k}, S. X. Li¹⁰, S. Y. Li⁵⁶, T. Li⁴⁵, W. D. Li^{1,58}, W. G. Li¹, X. H. Li^{66,53}, X. L. Li⁴⁵, Xiaoyu Li^{1,58}, Z. X. Li¹⁴, H. Liang^{66,53}, H. Liang^{1,58}, H. Liang³⁰, Y. F. Liang⁴⁹, Y. T. Liang^{28,58}, G. R. Liao¹³, L. Z. Liao⁴⁵, J. Libby²⁴, A. Limphirat⁵⁵, C. X. Lin⁵⁴, D. X. Lin^{28,58}, T. Lin¹, B. J. Liu¹, C. X. Liu¹, D. Liu^{17,66}, F. H. Liu⁴⁸, Fang Liu¹, Feng Liu⁶, G. M. Liu^{51,i}, H. Liu^{34,j,k}, H. B. Liu¹⁴, H. M. Liu^{1,58}, Huanhuan Liu¹, Huihui Liu¹⁹, J. B. Liu^{66,53}, J. L. Liu⁶⁷, J. Y. Liu^{1,58}, K. Liu¹, K. Y. Liu³⁶, Ke Liu²⁰, L. Liu^{66,53}, Lu Liu³⁹, M. H. Liu^{10,f}, P. L. Liu¹, Q. Liu⁵⁸, S. B. Liu^{66,53}, T. Liu^{10,f}, W. K. Liu³⁹, W. M. Liu^{66,53}, X. Liu^{34,j,k}, Y. Liu^{34,j,k}, Y. B. Liu³⁹, Z. A. Liu^{1,53,58}, Z. Q. Liu⁴⁵, X. C. Lou^{1,53,58}, F. X. Lu⁵⁴, H. J. Lu²¹, J. G. Lu^{1,53}, X. L. Lu¹, Y. Lu⁷, Y. P. Lu^{1,53}, Z. H. Lu¹, C. L. Luo³⁷, M. X. Luo⁷⁴, T. Luo^{10,f}, X. L. Luo^{1,53}, X. R. Lyu⁵⁸, Y. F. Lyu³⁹, F. C. Ma³⁶, H. L. Ma¹, L. L. Ma⁴⁵, M. M. Ma^{1,58}, Q. M. Ma¹, R. Q. Ma^{1,58}, R. T. Ma⁵⁸, X. Y. Ma^{1,53}, Y. Ma^{42,g}, F. E. Maas¹⁷, M. Maggiora^{69A,69C}, S. Maldaner⁴, S. Malde⁶⁴, Q. A. Malik⁶⁸, A. Mangoni^{26B}, Y. J. Mao^{42,g}, Z. P. Mao¹, S. Marcello^{69A,69C}, Z. X. Meng⁶¹, G. Mezzadri^{27A}, H. Miao¹, T. J. Min³⁸, R. E. Mitchell²⁵, X. H. Mo^{1,53,58}, N. Yu. Muchnoi^{11,b}, Y. Nefedov³², F. Nerling^{17,d}, I. B. Nikolaev^{11,b}, Z. Ning^{1,53}, S. Nisar^{9,l}, Y. Niu⁴⁵, S. L. Olsen⁵⁸, Q. Ouyang^{1,53,58}, S. Pacetti^{26B,26C}, X. Pan^{10,f}, Y. Pan⁵², A. Pathak³⁰, M. Pelizaeus⁴, H. P. Peng^{66,53}, K. Peters^{12,d}, J. L. Ping³⁷, R. G. Ping^{1,58}, S. Plura³¹, S. Pogodin³², V. Prasad^{66,53}, F. Z. Qi¹, H. Qi^{66,53}, H. R. Qi⁵⁶, M. Qi³⁸, T. Y. Qi^{10,f}, S. Qian^{1,53}, W. B. Qian⁵⁸, Z. Qian⁵⁴, C. F. Qiao⁵⁸, J. J. Qin⁶⁷, L. Q. Qin¹³, X. P. Qin^{10,f}, X. S. Qin⁴⁵, Z. H. Qin^{1,53}, J. F. Qiu¹, S. Q. Qu⁵⁶, K. H. Rashid⁶⁸, C. F. Redmer³¹, K. J. Ren³⁵, A. Rivetti^{69C}, V. Rodin⁵⁹, M. Rolo^{69C}, G. Rong^{1,58}, Ch. Rosner¹⁷, S. N. Ruan³⁹, H. S. Sang⁶⁶, A. Sarantsev^{32,c}, Y. Schelhaas³¹, C. Schner⁴, K. Schoenning⁷⁰, M. Scodreggio^{27A,27B}, K. Y. Shan^{10,f}, W. Shan²², X. Y. Shan^{66,53}, J. F. Shangguan⁵⁰, L. G. Shao^{1,58}, M. Shao^{66,53}, C. P. Shen^{10,f}, H. F. Shen^{1,58}, X. Y. Shen^{1,58}, B. A. Shi⁵⁸, H. C. Shi^{66,53}, J. Y. Shi¹, q. q. Shi⁵⁰, R. S. Shi^{1,58}, X. Shi^{1,53}, X. D. Shi^{66,53}, J. J. Song¹⁸, W. M. Song^{30,1}, Y. X. Song^{42,g}, S. Sosio^{69A,69C}, S. Spataro^{69A,69C}, F. Stierli³¹, K. X. Su⁷¹, P. P. Su⁵⁰, Y. J. Su⁵⁸, G. X. Sun¹, H. Sun⁵⁸, H. K. Sun¹, J. F. Sun¹⁸, L. Sun⁷¹, S. S. Sun^{1,58}, T. Sun^{1,58}, W. Y. Sun³⁰, X. Sun^{23,h}, Y. J. Sun^{66,53}, Y. Z. Sun¹, Z. T. Sun⁴⁵, Y. H. Tan⁷¹, Y. X. Tan^{66,53}, C. J. Tang⁴⁹, G. Y. Tang⁷¹, J. Tang⁵⁴, L. Y. Tao⁶⁷, Q. T. Tao^{23,h}, M. Tat⁶⁴, J. X. Teng^{66,53}, V. Thoren⁷⁰, W. H. Tian⁴⁷, Y. Tian^{28,58}, I. Uman^{57B}, B. Wang¹, B. L. Wang⁵⁸, C. W. Wang³⁸, D. Y. Wang^{42,g}, F. Wang⁶⁷, H. J. Wang^{34,j,k}, H. P. Wang^{1,58}, K. Wang^{1,53}, L. L. Wang¹, M. Wang⁴⁵, M. Z. Wang^{42,g}, Meng Wang^{1,58}, S. Wang¹³, S. Wang^{10,f}, T. Wang^{10,f}, T. J. Wang³⁹, W. Wang⁵⁴, W. H. Wang⁷¹, W. P. Wang^{66,53}, X. Wang^{42,g}, X. F. Wang^{34,j,k}, X. L. Wang^{10,f}, Y. Wang⁵⁶, Y. D. Wang⁴¹, Y. F. Wang^{1,53,58}, Y. H. Wang⁴³, Y. Q. Wang¹, Yaqian Wang^{16,1}, Z. Wang^{1,53}, Z. Y. Wang^{1,58}, Ziyi Wang⁵⁸, D. H. Wei¹³, F. Weidner⁶³, S. P. Wen¹, D. J. White⁶², U. Wiedner⁴, G. Wilkinson⁶⁴, M. Wolke⁷⁰, L. Wollenberg⁴, J. F. Wu^{1,58}, L. H. Wu¹, L. J. Wu^{1,58}, X. Wu^{10,f}, X. H. Wu³⁰, Y. Wu⁶⁶, Z. Wu^{1,53}, L. Xia^{66,53}, T. Xiang^{42,g}, D. Xiao^{34,j,k}, G. Y. Xiao³⁸, H. Xiao^{10,f}, S. Y. Xiao¹, Y. L. Xiao^{10,f}, Z. J. Xiao³⁷, C. Xie³⁸, X. H. Xie^{42,g}, Y. Xie⁴⁵, Y. G. Xie^{1,53}, Y. H. Xie⁶, Z. P. Xie^{66,53}, T. Y. Xing^{1,58}, C. F. Xu¹, C. J. Xu⁵⁴, G. F. Xu¹, H. Y. Xu⁶¹, Q. J. Xu¹⁵, X. P. Xu⁵⁰, Y. C. Xu⁵⁸, Z. P. Xu³⁸, F. Yan^{10,f}, L. Yan^{10,f}, W. B. Yan^{66,53}, W. C. Yan⁷⁵, H. J. Yang^{46,e}, H. L. Yang³⁰, H. X. Yang¹, L. Yang⁴⁷, S. L. Yang⁵⁸, Tao Yang¹, Y. F. Yang³⁹, Y. X. Yang^{1,58}, Yifan Yang^{1,58}, M. Ye^{1,53}, M. H. Ye⁸, J. H. Yin¹, Z. Y. You⁵⁴, B. X. Yu^{1,53,58}, C. X. Yu³⁹, G. Yu^{1,58}, T. Yu⁶⁷, X. D. Yu^{42,g}, C. Z. Yuan^{1,58}, L. Yuan², S. C. Yuan¹, X. Q. Yuan¹, Y. Yuan^{1,58}, Z. Y. Yuan⁵⁴, C. X. Yue³⁵, A. A. Zafar⁶⁸, F. R. Zeng⁴⁵, X. Zeng⁶, Y. Zeng^{23,h}, Y. H. Zhan⁵⁴, A. Q. Zhang¹, B. L. Zhang¹, B. X. Zhang¹, D. H. Zhang³⁹, G. Y. Zhang¹⁸, H. Zhang⁶⁶, H. H. Zhang³⁰, H. H. Zhang⁵⁴, H. Y. Zhang^{1,53}, J. L. Zhang⁷², J. Q. Zhang³⁷, J. W. Zhang^{1,53,58}, J. X. Zhang^{34,j,k}, J. Y. Zhang¹, J. Z. Zhang^{1,58}, Jianyu Zhang^{1,58}, Jiawei Zhang^{1,58}, L. M. Zhang⁵⁶, L. Q. Zhang⁵⁴, Lei Zhang³⁸, P. Zhang¹, Q. Y. Zhang^{35,75}, Shuihan Zhang^{1,58},

Shulei Zhang^{23,h}, X. D. Zhang⁴¹, X. M. Zhang¹, X. Y. Zhang⁴⁵, X. Y. Zhang⁵⁰, Y. Zhang⁶⁴, Y. T. Zhang⁷⁵, Y. H. Zhang^{1,53}, Yan Zhang^{66,53}, Yao Zhang¹, Z. H. Zhang¹, Z. Y. Zhang⁷¹, Z. Y. Zhang³⁹, G. Zhao¹, J. Zhao³⁵, J. Y. Zhao^{1,58}, J. Z. Zhao^{1,53}, Lei Zhao^{66,53}, Ling Zhao¹, M. G. Zhao³⁹, Q. Zhao¹, S. J. Zhao⁷⁵, Y. B. Zhao^{1,53}, Y. X. Zhao^{28,58}, Z. G. Zhao^{66,53}, A. Zhemchugov^{32,a}, B. Zheng⁶⁷, J. P. Zheng^{1,53}, Y. H. Zheng⁵⁸, B. Zhong³⁷, C. Zhong⁶⁷, X. Zhong⁵⁴, H. Zhou⁴⁵, L. P. Zhou^{1,58}, X. Zhou⁷¹, X. K. Zhou⁵⁸, X. R. Zhou^{66,53}, X. Y. Zhou³⁵, Y. Z. Zhou^{10,f}, J. Zhu³⁹, K. Zhu¹, K. J. Zhu^{1,53,58}, L. X. Zhu⁵⁸, S. H. Zhu⁶⁵, S. Q. Zhu³⁸, T. J. Zhu⁷², W. J. Zhu^{10,f}, Y. C. Zhu^{66,53}, Z. A. Zhu^{1,58}, B. S. Zou¹, J. H. Zou¹

(BESIII Collaboration)

- ¹ *Institute of High Energy Physics, Beijing 100049, People's Republic of China*
² *Beihang University, Beijing 100191, People's Republic of China*
³ *Beijing Institute of Petrochemical Technology, Beijing 102617, People's Republic of China*
⁴ *Bochum Ruhr-University, D-44780 Bochum, Germany*
⁵ *Carnegie Mellon University, Pittsburgh, Pennsylvania 15213, USA*
⁶ *Central China Normal University, Wuhan 430079, People's Republic of China*
⁷ *Central South University, Changsha 410083, People's Republic of China*
⁸ *China Center of Advanced Science and Technology, Beijing 100190, People's Republic of China*
⁹ *COMSATS University Islamabad, Lahore Campus, Defence Road, Off Raiwind Road, 54000 Lahore, Pakistan*
¹⁰ *Fudan University, Shanghai 200433, People's Republic of China*
¹¹ *G.I. Budker Institute of Nuclear Physics SB RAS (BINP), Novosibirsk 630090, Russia*
¹² *GSF Helmholtzcentre for Heavy Ion Research GmbH, D-64291 Darmstadt, Germany*
¹³ *Guangxi Normal University, Guilin 541004, People's Republic of China*
¹⁴ *Guangxi University, Nanning 530004, People's Republic of China*
¹⁵ *Hangzhou Normal University, Hangzhou 310036, People's Republic of China*
¹⁶ *Hebei University, Baoding 071002, People's Republic of China*
¹⁷ *Helmholtz Institute Mainz, Staudinger Weg 18, D-55099 Mainz, Germany*
¹⁸ *Henan Normal University, Xinxiang 453007, People's Republic of China*
¹⁹ *Henan University of Science and Technology, Luoyang 471003, People's Republic of China*
²⁰ *Henan University of Technology, Zhengzhou 450001, People's Republic of China*
²¹ *Huangshan College, Huangshan 245000, People's Republic of China*
²² *Hunan Normal University, Changsha 410081, People's Republic of China*
²³ *Hunan University, Changsha 410082, People's Republic of China*
²⁴ *Indian Institute of Technology Madras, Chennai 600036, India*
²⁵ *Indiana University, Bloomington, Indiana 47405, USA*
²⁶ *INFN Laboratori Nazionali di Frascati, (A)INFN Laboratori Nazionali di Frascati, I-00044, Frascati, Italy; (B)INFN Sezione di Perugia, I-06100, Perugia, Italy; (C)University of Perugia, I-06100, Perugia, Italy*
²⁷ *INFN Sezione di Ferrara, (A)INFN Sezione di Ferrara, I-44122, Ferrara, Italy; (B)University of Ferrara, I-44122, Ferrara, Italy*
²⁸ *Institute of Modern Physics, Lanzhou 730000, People's Republic of China*
²⁹ *Institute of Physics and Technology, Peace Avenue 54B, Ulaanbaatar 13330, Mongolia*
³⁰ *Jilin University, Changchun 130012, People's Republic of China*
³¹ *Johannes Gutenberg University of Mainz, Johann-Joachim-Becher-Weg 45, D-55099 Mainz, Germany*
³² *Joint Institute for Nuclear Research, 141980 Dubna, Moscow region, Russia*
³³ *Justus-Liebig-Universitaet Giessen, II. Physikalisches Institut, Heinrich-Buff-Ring 16, D-35392 Giessen, Germany*
³⁴ *Lanzhou University, Lanzhou 730000, People's Republic of China*
³⁵ *Liaoning Normal University, Dalian 116029, People's Republic of China*
³⁶ *Liaoning University, Shenyang 110036, People's Republic of China*
³⁷ *Nanjing Normal University, Nanjing 210023, People's Republic of China*
³⁸ *Nanjing University, Nanjing 210093, People's Republic of China*
³⁹ *Nankai University, Tianjin 300071, People's Republic of China*
⁴⁰ *National Centre for Nuclear Research, Warsaw 02-093, Poland*
⁴¹ *North China Electric Power University, Beijing 102206, People's Republic of China*
⁴² *Peking University, Beijing 100871, People's Republic of China*
⁴³ *Qufu Normal University, Qufu 273165, People's Republic of China*
⁴⁴ *Shandong Normal University, Jinan 250014, People's Republic of China*
⁴⁵ *Shandong University, Jinan 250100, People's Republic of China*
⁴⁶ *Shanghai Jiao Tong University, Shanghai 200240, People's Republic of China*
⁴⁷ *Shanxi Normal University, Linfen 041004, People's Republic of China*
⁴⁸ *Shanxi University, Taiyuan 030006, People's Republic of China*
⁴⁹ *Sichuan University, Chengdu 610064, People's Republic of China*
⁵⁰ *Soochow University, Suzhou 215006, People's Republic of China*
⁵¹ *South China Normal University, Guangzhou 510006, People's Republic of China*
⁵² *Southeast University, Nanjing 211100, People's Republic of China*
⁵³ *State Key Laboratory of Particle Detection and Electronics, Beijing 100049, Hefei 230026, People's Republic of China*

- ⁵⁴ Sun Yat-Sen University, Guangzhou 510275, People's Republic of China
- ⁵⁵ Suranaree University of Technology, University Avenue 111, Nakhon Ratchasima 30000, Thailand
- ⁵⁶ Tsinghua University, Beijing 100084, People's Republic of China
- ⁵⁷ Turkish Accelerator Center Particle Factory Group, (A)Istinye University, 34010, Istanbul, Turkey; (B)Near East University, Nicosia, North Cyprus, Mersin 10, Turkey
- ⁵⁸ University of Chinese Academy of Sciences, Beijing 100049, People's Republic of China
- ⁵⁹ University of Groningen, NL-9747 AA Groningen, The Netherlands
- ⁶⁰ University of Hawaii, Honolulu, Hawaii 96822, USA
- ⁶¹ University of Jinan, Jinan 250022, People's Republic of China
- ⁶² University of Manchester, Oxford Road, Manchester, M13 9PL, United Kingdom
- ⁶³ University of Muenster, Wilhelm-Klemm-Strasse 9, 48149 Muenster, Germany
- ⁶⁴ University of Oxford, Keble Road, Oxford OX13RH, United Kingdom
- ⁶⁵ University of Science and Technology Liaoning, Anshan 114051, People's Republic of China
- ⁶⁶ University of Science and Technology of China, Hefei 230026, People's Republic of China
- ⁶⁷ University of South China, Hengyang 421001, People's Republic of China
- ⁶⁸ University of the Punjab, Lahore-54590, Pakistan
- ⁶⁹ University of Turin and INFN, (A)University of Turin, I-10125, Turin, Italy; (B)University of Eastern Piedmont, I-15121, Alessandria, Italy; (C)INFN, I-10125, Turin, Italy
- ⁷⁰ Uppsala University, Box 516, SE-75120 Uppsala, Sweden
- ⁷¹ Wuhan University, Wuhan 430072, People's Republic of China
- ⁷² Xinyang Normal University, Xinyang 464000, People's Republic of China
- ⁷³ Yunnan University, Kunming 650500, People's Republic of China
- ⁷⁴ Zhejiang University, Hangzhou 310027, People's Republic of China
- ⁷⁵ Zhengzhou University, Zhengzhou 450001, People's Republic of China
- ^a Also at the Moscow Institute of Physics and Technology, Moscow 141700, Russia
- ^b Also at the Novosibirsk State University, Novosibirsk, 630090, Russia
- ^c Also at the NRC "Kurchatov Institute", PNPI, 188300, Gatchina, Russia
- ^d Also at Goethe University Frankfurt, 60323 Frankfurt am Main, Germany
- ^e Also at Key Laboratory for Particle Physics, Astrophysics and Cosmology, Ministry of Education; Shanghai Key Laboratory for Particle Physics and Cosmology; Institute of Nuclear and Particle Physics, Shanghai 200240, People's Republic of China
- ^f Also at Key Laboratory of Nuclear Physics and Ion-beam Application (MOE) and Institute of Modern Physics, Fudan University, Shanghai 200443, People's Republic of China
- ^g Also at State Key Laboratory of Nuclear Physics and Technology, Peking University, Beijing 100871, People's Republic of China
- ^h Also at School of Physics and Electronics, Hunan University, Changsha 410082, China
- ⁱ Also at Guangdong Provincial Key Laboratory of Nuclear Science, Institute of Quantum Matter, South China Normal University, Guangzhou 510006, China
- ^j Also at Frontiers Science Center for Rare Isotopes, Lanzhou University, Lanzhou 730000, People's Republic of China
- ^k Also at Lanzhou Center for Theoretical Physics, Lanzhou University, Lanzhou 730000, People's Republic of China
- ^l Also at the Department of Mathematical Sciences, IBA, Karachi, Pakistan

A measurement of the CP -even fraction of the decay $D^0 \rightarrow \pi^+\pi^-\pi^+\pi^-$ is performed with a quantum-correlated $\psi(3770) \rightarrow D\bar{D}$ data sample collected by the BESIII experiment, corresponding to an integrated luminosity of 2.93 fb^{-1} . Using a combination of CP eigenstates, $D \rightarrow \pi^+\pi^-\pi^0$ and $D \rightarrow K_{S,L}^0\pi^+\pi^-$ as tagging modes, the CP -even fraction is measured to be $F_+^{4\pi} = 0.735 \pm 0.015 \pm 0.005$, where the first uncertainty is statistical and the second is systematic. This is the most precise determination of this quantity to date. It provides valuable model-independent input for the measurement of the CKM angle γ with $B^\pm \rightarrow DK^\pm$ decays, and for time-dependent studies of CP violation and mixing in the D^0 - \bar{D}^0 system.

I. INTRODUCTION

Studies of CP violation in the heavy-quark sector can improve our understanding of the weak interaction and probe for new effects that cannot be accommodated within the Standard Model of particle physics. Many of these studies use neutral charm mesons, with a particular case of interest being when the charm meson decays to a CP eigenstate. Observables in the process $B^\pm \rightarrow DK^\pm$, where the D is a superposition of D^0 and \bar{D}^0 and is here reconstructed in a CP eigenstate, are sensitive to

the CKM angle γ , and thus allow for tests of the Standard Model description of CP violation [1, 2]. Furthermore, measurements of the decay time of charm mesons produced in a known flavor eigenstate and reconstructed in a CP eigenstate bring information on D^0 - \bar{D}^0 oscillations [3]. These strategies can be extended to so-called quasi CP eigenstates: self-conjugate multi-body decays that are not themselves CP eigenstates, but dominated by intermediate states of definite CP [4, 5]. The parameter F_+ quantifies the fractional CP -even content of these modes, with $F_+ = 1$ (0) corresponding to a pure CP -even

(-odd) final state. Measurements using these quasi CP eigenstates require good knowledge of F_+ for interpreting the results.

CP -even fractions and other parameters associated with the strong dynamics of charm-meson decays are preferentially measured from data collected at the $\psi(3770)$ resonance. The quantum correlation between the two charm mesons produced from the decay of the $\psi(3770)$ gives rise to interference effects that provide access to these parameters. This approach has the benefit of being model-independent and is to be contrasted with alternative strategies that are based on amplitude models constructed from decays of mesons produced in incoherent environments [6, 7]. Measurements of the CP -even fraction with correlated $D\bar{D}$ pairs have been performed with data collected by the CLEO-c experiment for a range of decay modes including $D \rightarrow \pi^+\pi^-\pi^+\pi^-$ [4, 8–10].

The decay $D \rightarrow \pi^+\pi^-\pi^+\pi^-$ is an attractive mode for CP -violation studies on account of its reasonably high branching fraction and the good reconstruction efficiency that both LHCb and Belle II have for the fully charged final state [11, 12]. This paper presents a determination of the CP -even fraction, $F_+^{4\pi}$, of this decay using quantum-correlated $\psi(3770) \rightarrow D\bar{D}$ data collected by the BESIII experiment, corresponding to an integrated luminosity of 2.93 fb^{-1} . It is the first measurement of a CP -even fraction with this data set, although BESIII has presented studies of other hadronic parameters performed with correlated $D\bar{D}$ pairs in a variety of channels [13–17].

II. MEASUREMENT METHOD

The strong decay $\psi(3770) \rightarrow D\bar{D}$ conserves the negative C quantum number, leaving the charm-meson pair in an overall P -wave state. The quantum correlation between the two mesons in this antisymmetric wavefunction provides the opportunity to determine the CP -even fraction of $D^0 \rightarrow \pi^+\pi^-\pi^+\pi^-$. (The parameter for the \bar{D}^0 decay is identical.)

The method adopted in this analysis is similar to that applied in previous measurements [4, 8, 10], and is based on samples of ‘double-tag’ (DT) and ‘single-tag’ (ST) events. The DT events are those where one D meson decays to the signal final-state $\pi^+\pi^-\pi^+\pi^-$ and the \bar{D} meson decays to a ‘tag mode’. The ST events are those where only one charm meson is reconstructed in its decay to a tag mode.

Various classes of tag modes are employed, the first ones being pure CP eigenstates. Several decays involving K_S^0 and K_L^0 mesons are included in this category, as CP violation in the kaon system can be neglected at the current level of experimental precision. The same consideration applies to CP violation associated with the

charm mesons themselves [18]. For a CP -tag mode, here denoted as f , the predicted DT yield is given by

$$M(4\pi, f) = 2N_{D\bar{D}}\mathcal{B}(4\pi)\mathcal{B}(f)\epsilon_{DT}[1 - \eta_{CP}^f(2F_+^{4\pi} - 1)], \quad (1)$$

where $N_{D\bar{D}}$ is the number of neutral charm-meson pairs in the sample, $\mathcal{B}(X)$ is the branching fraction of $D \rightarrow X$, ϵ_{DT} is the DT reconstruction efficiency of the event, and η_{CP}^f is the CP -eigenvalue (+1 or -1) of the tag channel f . In this and subsequent expressions, terms of $\mathcal{O}(y^2)$ in the charm mixing parameter $y = (0.615_{-0.055}^{+0.056})\%$ [18] are neglected.

The predicted ST yield is given by

$$S(f) = 2N_{D\bar{D}}\mathcal{B}(f)\epsilon_{ST}[1 - \eta_{CP}^f y], \quad (2)$$

where ϵ_{ST} is the reconstruction efficiency of the ST decay. Then $F_+^{4\pi}$ can be accessed through

$$F_+^{4\pi} = \frac{N^+}{N^+ + N^-}, \quad (3)$$

where N^+ , which measures the proportion of CP -even D mesons that decay to $\pi^+\pi^-\pi^+\pi^-$, is $M(4\pi, f)[1 - \eta_{CP}^f y]/S(f)$ for a CP -odd tag, and N^- is the analogous quantity for a CP -even tag. Experimentally, N^+ and N^- are determined from the corresponding ratios involving the measured DT and ST yields and are averaged over all employed tags. This calculation assumes that the DT-event efficiency can be factorized into the ST efficiency and the reconstruction efficiency of the signal decay and that any corrections to this assumption are common to all classes of DT. Possible exceptions to these assumptions are examined in the assignment of systematic uncertainties. Modifications to this procedure, described in Sec. IV, are required for certain classes of tag involving K_L^0 mesons where the ST yields cannot be directly measured.

A specific tag used in the analysis is $D \rightarrow \pi^+\pi^-\pi^0$, which is a quasi CP eigenstate. Here the predicted DT yield is given by

$$M(4\pi, f) = 2N_{D\bar{D}}\mathcal{B}(4\pi)\mathcal{B}(\pi\pi\pi^0)\epsilon_{DT}[1 - (2F_+^{\pi\pi\pi^0} - 1)(2F_+^{4\pi} - 1)], \quad (4)$$

where $F_+^{\pi\pi\pi^0} = 0.973 \pm 0.017$ is the CP -even fraction of the tag mode [8], and the predicted ST yield is

$$S(\pi\pi\pi^0) = 2N_{D\bar{D}}\mathcal{B}(\pi\pi\pi^0)\epsilon_{ST}[1 - (2F_+^{\pi\pi\pi^0} - 1)y]. \quad (5)$$

In this case, $F_+^{4\pi}$ can be accessed through the ratio

$$F_+^{4\pi} = \frac{N^+ F_+^{\pi\pi\pi^0}}{N^{\pi\pi\pi^0} - N^+ + 2N^+ F_+^{\pi\pi\pi^0}}, \quad (6)$$

with $N^{\pi\pi\pi^0} = M(4\pi, \pi\pi\pi^0)[1 - (2F_+^{\pi\pi\pi^0} - 1)y]/S(\pi\pi\pi^0)$. Experimentally, N^+ and $N^{\pi\pi\pi^0}$ are again determined from the measured DT and ST yields, with the same assumptions concerning the factorization of the DT-event efficiency as discussed above.

The self-conjugate decays $D \rightarrow K_S^0\pi^+\pi^-$ and $D \rightarrow K_L^0\pi^+\pi^-$ are known to have CP -even fractions close to 0.5 [19], and hence would give poor sensitivity to $F_+^{4\pi}$ if used as a global tag in an analogous manner to $D \rightarrow \pi^+\pi^-\pi^0$. However, a local measurement may be performed where the position of the tag decay in its phase space is considered. This is possible because studies on the variation in the strong-phase difference between the D^0 and \bar{D}^0 amplitudes across the Dalitz plot have been performed for these modes. In particular, measurements exist of the amplitude-weighted cosine of the average strong-phase difference in binned regions of phase space [14, 15, 20]. The predicted DT yields in bin i are given by

$$\begin{aligned} M_i(4\pi, K_S^0\pi^+\pi^-) &= \\ H[K_i + K_{-i} - 2\sqrt{K_i K_{-i}}c_i(2F_+^{4\pi} - 1)], \\ M'_i(4\pi, K_L^0\pi^+\pi^-) &= \\ H'[K'_i + K'_{-i} + 2\sqrt{K'_i K'_{-i}}c'_i(2F_+^{4\pi} - 1)], \end{aligned} \quad (7)$$

where H and H' are normalization factors, K_i (K'_i) is the fractional rate of D^0 decays to $K_S^0\pi^+\pi^-$ ($K_L^0\pi^+\pi^-$) in the i -th bin, and c_i (c'_i) is the amplitude-weighted cosine of the average strong-phase difference in the i -th bin. When comparing the observed distribution of events throughout the bins with the predictions, there is no need to know the overall efficiency scale. However, it is important to account for relative variations in DT efficiency bin-to-bin as well as migration effects brought about by bin misassignments.

III. BESIII DETECTOR AND MONTE CARLO SIMULATION

The BESIII detector [21] records symmetric e^+e^- collisions provided by the BEPCII storage ring [22], which operates with a peak luminosity of $1 \times 10^{33} \text{ cm}^{-2}\text{s}^{-1}$ in the center-of-mass energy range from 2.0 to 4.95 GeV. BESIII has collected large data samples in this energy region [23]. The cylindrical core of the BESIII detector covers 93% of the full solid angle and consists of a helium-based multilayer drift chamber (MDC), a plastic scintillator time-of-flight system (TOF), and a CsI(Tl) electromagnetic calorimeter (EMC), which are all enclosed in a superconducting solenoidal magnet providing a 1.0 T magnetic field. The solenoid is supported by an octagonal flux-return yoke with resistive plate counter muon-identification modules interleaved with steel. The charged-particle momentum resolution at 1 GeV/ c is 0.5%, and the dE/dx resolution is 6% for electrons from

Bhabha scattering. The EMC measures photon energies with a resolution of 2.5% (5%) at 1 GeV in the barrel (end-cap) region. The time resolution in the TOF barrel region is 68 ps, while that in the end-cap region is 110 ps.

Simulated samples, which are produced with the GEANT4-based [24] Monte Carlo (MC) package that includes the description of the detector geometry and response, are used to determine the detection efficiencies and estimate the backgrounds. The beam-energy spread of 0.97 MeV and the initial-state radiation (ISR) in the e^+e^- annihilations, which is modeled with the generator KKMC [25], are included in the simulation. The inclusive MC samples for background studies consist of the production of neutral and charged charm-meson pairs from $\psi(3770)$ decays, decays of the $\psi(3770)$ to charmonia or light hadrons, the ISR production of the J/ψ and $\psi(3770)$ states, continuum processes, and the QED processes $e^+e^- \rightarrow e^+e^-$, $e^+e^- \rightarrow \mu^+\mu^-$ and $e^+e^- \rightarrow \tau^+\tau^-$. No attempt is made to include quantum-correlation effects in $\psi(3770) \rightarrow D\bar{D}$ decays in the inclusive MC sample. The equivalent integrated luminosity of the inclusive MC samples is about 10 times that of the data, apart from the production of $D\bar{D}$ events, where the equivalent integrated luminosity is about 20 times that of the data. All particle decays are modeled with EVTGEN [26] using branching fractions either taken from the Particle Data Group [27], when available, or otherwise estimated with LUNDCHARM [28, 29]. The final-state radiation from the charged final-state particles is incorporated with the PHOTOS package [30].

Signal MC samples of around 200,000 events are generated separately for the different tag channels. In this generation, the $D \rightarrow \pi^+\pi^-\pi^+\pi^-$ decay follows an isobar-based amplitude model fitted to a BESIII sample of these decays, where the flavor of the decaying meson is inferred by reconstructing the other charm meson in the event through its decay into a flavor-specific final state. The model contains the main resonant structures observed in data. The simulated DT samples involving $D \rightarrow K_{S,L}^0\pi^+\pi^-$ tags are an order of magnitude larger in size and the tag decays are implemented with an amplitude model developed by the BaBar collaboration [31]. In all the DT samples, quantum correlations are included in the generation to ensure the best possible description of the reconstruction efficiency, especially for the different bins of phase space of the $K_{S,L}^0\pi^+\pi^-$ tag modes.

IV. EVENT SELECTION AND YIELD DETERMINATION

Table I lists the tag categories that are employed in the analysis: CP -even eigenstates, CP -odd eigenstates, the quasi- CP -even mode $D \rightarrow \pi^+\pi^-\pi^0$, and the self-conjugate decays $D \rightarrow K_{S,L}^0\pi^+\pi^-$ of mixed CP that are analyzed in bins of phase space. The final-state resonances are reconstructed in the following channels:

$K_S^0 \rightarrow \pi^+\pi^-$, $\pi^0 \rightarrow \gamma\gamma$, $\eta \rightarrow \gamma\gamma$ and $\pi^+\pi^-\pi^0$, $\omega \rightarrow \pi^+\pi^-\pi^0$, and $\eta' \rightarrow \pi^+\pi^-\eta$ and $\gamma\pi^+\pi^-$.

TABLE I: Summary of tag channels.

Category	Decay modes
<i>CP</i> -even	K^+K^- , $K_S^0\pi^0\pi^0$, $K_L^0\pi^0$, $K_L^0\omega$
<i>CP</i> -odd	$K_S^0\pi^0$, $K_S^0\eta$, $K_S^0\eta'$, $K_S^0\omega$, $K_L^0\pi^0\pi^0$
Quasi <i>CP</i> -even	$\pi^+\pi^-\pi^0$
Mixed <i>CP</i>	$K_S^0\pi^+\pi^-$, $K_L^0\pi^+\pi^-$

DT events formed of tags involving a K_L^0 are partially reconstructed using a missing-mass technique. All other classes of DT events are fully reconstructed, as are ST events that do not contain a K_L^0 meson.

A. Basic event selection

Several basic requirements are imposed to ensure the quality of charged tracks in the analysis. Those tracks from K_S^0 candidates must lie within 20 cm of e^+e^- interaction point (IP) along the z -axis, which is the symmetry axis of the MDC. All other tracks must have a point of closest approach to the IP within ± 10 cm along the z -axis and 1 cm in the transverse plane. The polar angle θ with respect to the axis of the drift chamber must satisfy the condition $|\cos\theta| < 0.93$. Charged pions and kaons are distinguished by combining the information of the flight time measured from the TOF and the dE/dx measured in the MDC. The corresponding probabilities P_K (P_π) for the K (π) hypothesis are calculated and the track is labeled as a K (π) candidate if $P_K > P_\pi$ ($P_K < P_\pi$).

The photon candidates are reconstructed from the showers in EMC, with the energy required to be larger than 25 MeV for barrel showers ($|\cos\theta| < 0.80$) and 50 MeV for end-cap showers ($0.86 < |\cos\theta| < 0.92$). To suppress electronic noise or activity unrelated to the events, the time of the cluster measured from the EMC is required to be within 0 and 700 ns after the event start time. Furthermore, to eliminate showers originating from charged tracks, the angle subtended by the EMC shower and the position of the closest charged track at the EMC must be greater than 20 degrees as measured from the IP.

The K_S^0 candidates are reconstructed from pairs of tracks with opposite charge on which no particle-identification requirements are imposed. A fit is applied to constrain the track pair to a common vertex. The flight significance L/σ_L is required to be larger than 2, where L is the flight distance and σ_L is the corresponding standard deviation. In addition, the invariant mass is required to be within [0.487,0.511] GeV/ c^2 .

Pairs of photons are used to reconstruct $\pi^0(\eta)$ candidates, where the invariant mass of the pair must lie within [0.115, 0.150] ([0.480, 0.580]) GeV/ c^2 and at least one photon candidate is from the barrel region. In order to improve the momentum resolution, a kinematic fit is performed, where the reconstructed $\pi^0(\eta)$ invariant mass is constrained to the known value [27], and the fitted momentum of the $\pi^0(\eta)$ is used in the subsequent stages of the analysis. When reconstructing $\eta \rightarrow \pi^+\pi^-\pi^0$ decays, the invariant mass of the η candidate is required to be within [0.530, 0.565] GeV/ c^2 . Similarly, when reconstructing $\omega \rightarrow \pi^+\pi^-\pi^0$, $\eta' \rightarrow \pi^+\pi^-\eta(\gamma\gamma)$ and $\eta' \rightarrow \gamma\pi^+\pi^-$, the invariant mass is required to lie within [0.750,0.820], [0.940, 0.976] and [0.940, 0.970] GeV/ c^2 , respectively.

B. ST event selection and yields

ST events that do not contain a K_L^0 meson are reconstructed from the charged pion, charged kaon, K_S^0 , and resonance candidates. To suppress the combinatorial background, the energy difference, $\Delta E = E_D - \sqrt{s}/2$, is required to be within $\pm 3\sigma_{\Delta E}$ of the ΔE peak, where E_D is the measured energy of the D -meson candidate in the center-of-mass frame, \sqrt{s} is the center-of-mass energy, and $\sigma_{\Delta E}$ is the resolution of the ΔE distribution. To suppress background from cosmic and Bhabha events in the tag channel $D \rightarrow K^+K^-$, the two charged tracks must have a TOF time difference of less than 5 ns, and the further requirement that neither track is identified as an electron or a muon is applied. To suppress $D \rightarrow K_S^0\pi^0$ contamination in the selection of $D \rightarrow \pi^+\pi^-\pi^0$ decays, a K_S^0 -veto is applied, in which the event is rejected if the charged pion pair has a significant flight distance ($L/\sigma_L > 2$) and invariant mass lying within the range [0.481, 0.514]GeV/ c^2 . This use of flight-distance information is preferred to removing all events within the K_S^0 mass window as the *CP*-even fraction of this mode is only known for the full phase space of the decay [8].

In order to determine the ST yields for the *CP* eigenstate and quasi-*CP* eigenstate tags, the beam-constrained mass, $m_{BC} = \sqrt{(\sqrt{s}/2)^2 - |\mathbf{p}_D|^2}$, is used to identify the signal, where \mathbf{p}_D is the three-momentum vector of the D candidate in the center-of-mass frame. Binned maximum-likelihood fits are performed on the m_{BC} distributions, as shown in Fig. 1, where the signal is described by the shape found in MC simulation convolved with a Gaussian function, to account for differences in resolution between MC and data, and the combinatorial background is described by an ARGUS function with an end-point fixed to $\sqrt{s}/2$ [32]. The peaking-background contributions from other charm decays are estimated from MC simulation and then subtracted from the fitted ST yields. In the case of $D \rightarrow K_S^0\omega$, $K_S^0\eta\pi\pi^0$, and $K_S^0\eta'\gamma\pi\pi$, the peaking-background fractions are 11.5%, 9.7%, and 3.9%, respectively, and arise mainly from $D \rightarrow$

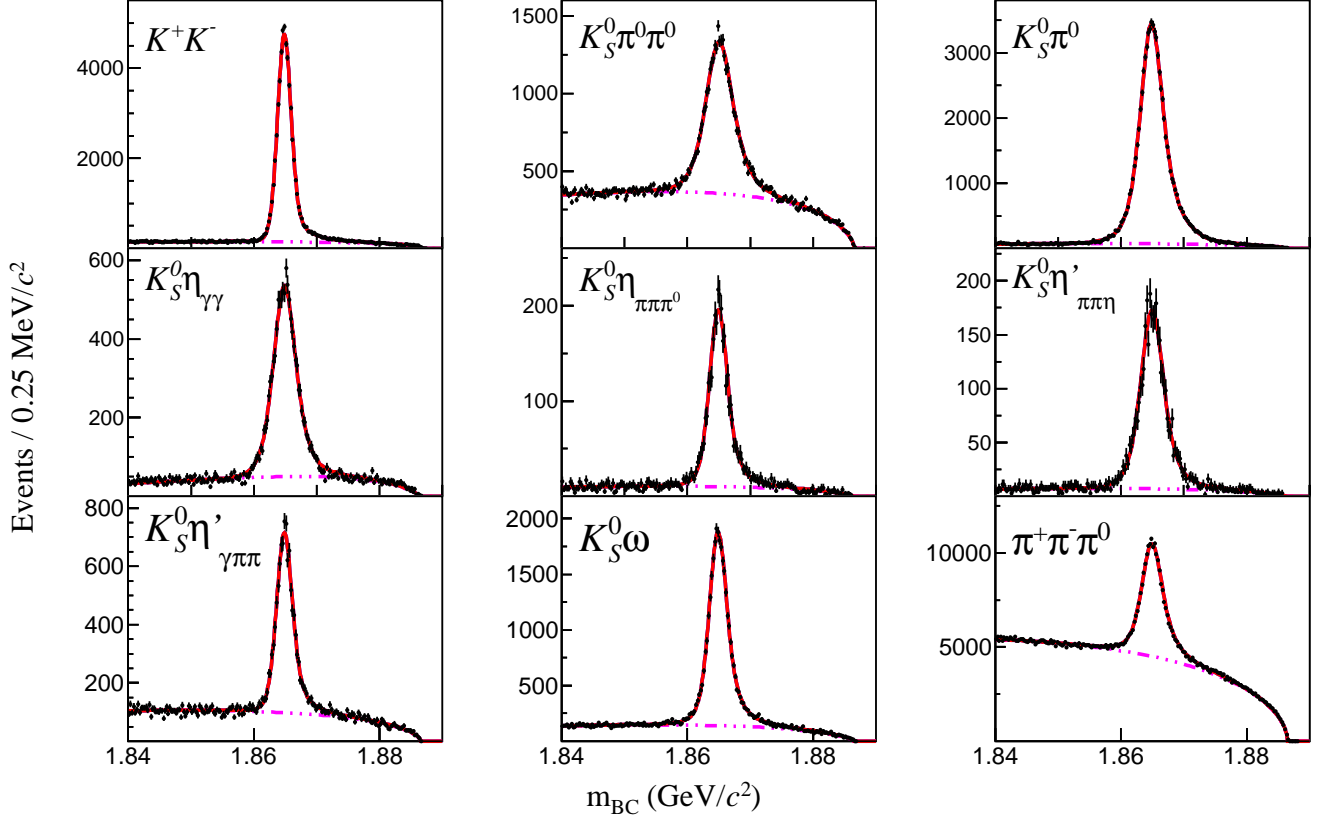


FIG. 1: Distributions of m_{BC} and fits used to determine the ST yields. In each plot the black dots with error bar are data, the total fit result is shown as the red solid line and the continuum background is shown as the pink dashed line.

$K_S^0 \pi^+ \pi^- \pi^0$ decays. The peaking-background fraction in the $D \rightarrow \pi^+ \pi^- \pi^0$ sample is 5%, mainly from $D \rightarrow K_S^0 \pi^0$ decays. The contamination in the $D \rightarrow K_S^0 \pi^0 (\pi^0)$ selection mainly comes from $D \rightarrow \pi^+ \pi^- \pi^0 (\pi^0)$ decays and constitutes 0.3% (3.1%) of the sample. For the other three channels, the peaking-background are not significant. The ST yields after background subtraction, N_{ST} , are summarized in Table II, together with the ΔE window imposed for each channel.

The difficulty of reconstructing K_L^0 mesons means that it is impractical to select ST samples for the modes $D \rightarrow K_L^0 X$ ($X = \omega, \pi^0$, or $\pi^0 \pi^0$). However, effective ST yields can be determined through the relation

$$N_{ST}(K_L^0 X) = 2N_{D\bar{D}} \mathcal{B}(K_L^0 X) \epsilon'_{ST}(K_L^0 X), \quad (8)$$

where $N_{ST}(K_L^0 X)$ is the effective ST yield for mode $D \rightarrow K_L^0 X$, $N_{D\bar{D}} = (10597 \pm 28 \pm 98) \times 10^3$ is the number of neutral charm-meson pairs in the sample [33] and $\mathcal{B}(K_L^0 X)$ is the branching fraction of the $D \rightarrow K_L^0 X$ mode [34]. The effective efficiency $\epsilon'_{ST}(K_L^0 X)$ is defined as the ratio of the efficiency for reconstructing $D \rightarrow \pi^+ \pi^- \pi^+ \pi^-$ versus $D \rightarrow K_L^0 X$ DT events with the partial-reconstruction technique, as discussed below, and the reconstruction efficiency for $D \rightarrow \pi^+ \pi^- \pi^+ \pi^-$. The effective ST yields are included in Table II.

C. DT event selection and yields

DT samples are selected for all tags not involving a K_L^0 by attempting to reconstruct the $D \rightarrow \pi^+ \pi^- \pi^+ \pi^-$ signal decay from the remaining tracks in the ST samples. Only events with four extra charged tracks are considered. All four charged tracks must be identified as pions and their net charge is required to be zero. A tight K_S^0 veto is applied to suppress background from $D \rightarrow K_S^0 \pi^+ \pi^-$ decays: if the invariant mass of any of the $\pi^+ \pi^-$ pairs lies within $[0.481, 0.514] \text{ GeV}/c^2$, the event is rejected. As this requirement removes a specific region of phase space, rejecting around 13% of the signal, it has the potential to bias the CP -even fraction of the sample. This effect is considered in the assignment of systematic uncertainties. The energy difference ΔE of the signal decay is required to lie within $[-0.026, 0.023] \text{ GeV}$.

For each fully reconstructed DT channel, the DT yield is determined by an unbinned maximum-likelihood fit to the m_{BC} distribution of the signal D candidate. The m_{BC} distributions and the fits for the CP eigenstate and quasi- CP eigenstate tags are presented in Fig. 2. In these fits, the signal is described by the MC-simulated shape convolved with a Gaussian function, and the combinato-

rial background is described by an ARGUS function. The fitted signal yield includes contamination from peaking-background contributions. The most significant source of peaking background is the residual contamination from $D \rightarrow K_S^0 \pi^+ \pi^-$ decays in the selection of the signal channel. The size of this background is determined from data by performing fits to the invariant-mass distribution of $\pi^+ \pi^-$ pairs associated with the signal candidate without any K_S^0 veto in place. The results are then scaled by the suppression factor of the veto on the background mode, as determined from the MC simulation. This background is found to vary from 2% to 5%, depending on the tag mode. The size of the other peaking backgrounds, such as $D \rightarrow K_S^0 \pi^0$ in the $D \rightarrow \pi^+ \pi^- \pi^0$ tag, are estimated from MC simulation. Where necessary, corrections are applied to account for the quantum-correlated enhancements or suppressions that are not simulated in the inclusive simulation, according to the CP content of the background. The DT yields after background subtraction are summarized in Table II.

DT channels involving a $D \rightarrow K_L^0 X$ tag mode cannot be fully reconstructed. Nonetheless, a partial reconstruction is performed, accounting for all other charged and neutral particles in the event, and the yield is determined using a missing-mass-squared technique. In this procedure the $D \rightarrow \pi^+ \pi^- \pi^+ \pi^-$ candidate is first reconstructed with the same criteria as used previously, and then the standard selections are imposed to select the remaining charged and neutral tracks in the event. Candidates for the tag modes $D \rightarrow K_L^0 \pi^0$, $D \rightarrow K_L^0 \pi^0 \pi^0$, $D \rightarrow K_L^0 \omega$, and $D \rightarrow K_L^0 \pi^+ \pi^-$ are selected from the charged tracks and π^0 candidates in the event. Any events with surplus charged tracks, surplus π^0 candidates, or an $\eta \rightarrow \gamma\gamma$ candidate are rejected. In the case of $D \rightarrow K_L^0 \omega$, events containing more than one ω candidate are discarded.

The signal yields in the partially reconstructed DTs are determined by performing unbinned maximum-likelihood fits to the squared missing-mass $M_{\text{miss}}^2 = (\sqrt{s}/2 - E_X)^2 - |\mathbf{p}_X + \hat{\mathbf{p}}_{4\pi} \sqrt{s/4 - M_D^2}|^2$, which is calculated in the center-of-mass frame. Here E_X and \mathbf{p}_X are the energy and three-momentum, respectively, of the reconstructed particles in the event not associated with the signal candidate, $\hat{\mathbf{p}}_{4\pi}$ is the direction of the signal candidate, and M_D is the known D^0 mass [27]. The M_{miss}^2 distributions and fits for the CP eigenstate tags are included in Fig. 2. The resulting signal yields can be found in Table II. In these fits, the signal distribution is described by the shape found in the MC simulation convolved with a Gaussian function whose width is a free parameter. Fixed contributions from MC simulation are included for peaking backgrounds, and the continuum background is modeled with a first-order Chebychev polynomial, whose parameters are determined in the fit. Peaking backgrounds arise mainly from $D \rightarrow K_S^0 \pi^+ \pi^-$ decays that are misreconstructed as $D \rightarrow \pi^+ \pi^- \pi^+ \pi^-$, or decays involving an unreconstructed K_S^0 meson that contaminate the tag candi-

dates. These backgrounds constitute 28%, 16%, and 7% of the $D \rightarrow K_L^0 \omega$, $K_L^0 \pi^0$, and $K_L^0 \pi^0 \pi^0$ samples, respectively.

TABLE II: Summary of ΔE requirements, ST yields (N_{ST}), and DT yields (N_{DT}) for each tag mode, grouped by tag category. The uncertainties are statistical. The entry ‘/’ indicates that the information is not defined (ΔE for $K_L^0 X$ modes) or not required for the analysis (ST yields for $K_{S,L}^0 \pi^+ \pi^-$).

Mode	ΔE (GeV)	N_{ST}	N_{DT}
$K^+ K^-$	[-0.021, 0.020]	56668±262	115.4±14.4
$K_S^0 \pi^0 \pi^0$	[-0.072, 0.053]	73176±299	36.4±10.3
$K_L^0 \pi^0$	/	79689±5631	130.9±18.8
$K_L^0 \omega$	/	29128±1962	61.5±13.8
$K_S^0 \pi^0$	[-0.071, 0.051]	73176±299	326.0±19.2
$K_S^0 \eta \gamma \gamma$	[-0.038, 0.036]	10071±123	57.7±7.7
$K_S^0 \eta \pi \pi \pi^0$	[-0.035, 0.028]	2775±65	16.5±4.2
$K_S^0 \eta' \pi \pi \eta$	[-0.035, 0.031]	3449±67	11.6±3.5
$K_S^0 \eta' \gamma \pi \pi$	[-0.031, 0.025]	8691±126	41.1±7.5
$K_S^0 \omega$	[-0.042, 0.033]	26220±215	128.7±13.8
$K_L^0 \pi^0 \pi^0$	/	25772±2184	178.5±23.9
$\pi^+ \pi^- \pi^0$	[-0.062, 0.051]	115556±682	190.7±24.6
$K_S^0 \pi^+ \pi^-$	[-0.026, 0.023]	/	539.7±26.0
$K_L^0 \pi^+ \pi^-$	/	/	1374.6±50.4

V. CP -EVEN FRACTION MEASUREMENT

The CP -even fraction is determined using the ST and DT yields of the CP -eigenstate and quasi- CP -eigenstate tags, and the distribution of decays in tag phase space of the $D \rightarrow K_{S,L}^0 \pi^+ \pi^-$ DT events. The analysis follows the procedure outlined in Sec. II.

A. CP -eigenstate tags

The N^+ and N^- parameters are determined for each tag channel, and systematic uncertainties are assigned as discussed in Sec. VD. The results are displayed in Fig. 3. A least-squares fit, which takes account of the correlations between the systematic uncertainties, returns

$$\begin{aligned} \langle N^+ \rangle &= (4.73 \pm 0.20 \pm 0.09) \times 10^{-3}, \\ \langle N^- \rangle &= (1.83 \pm 0.16 \pm 0.04) \times 10^{-3}, \end{aligned}$$

where, here and for all subsequent results, the first uncertainty is statistical and the second is systematic. The

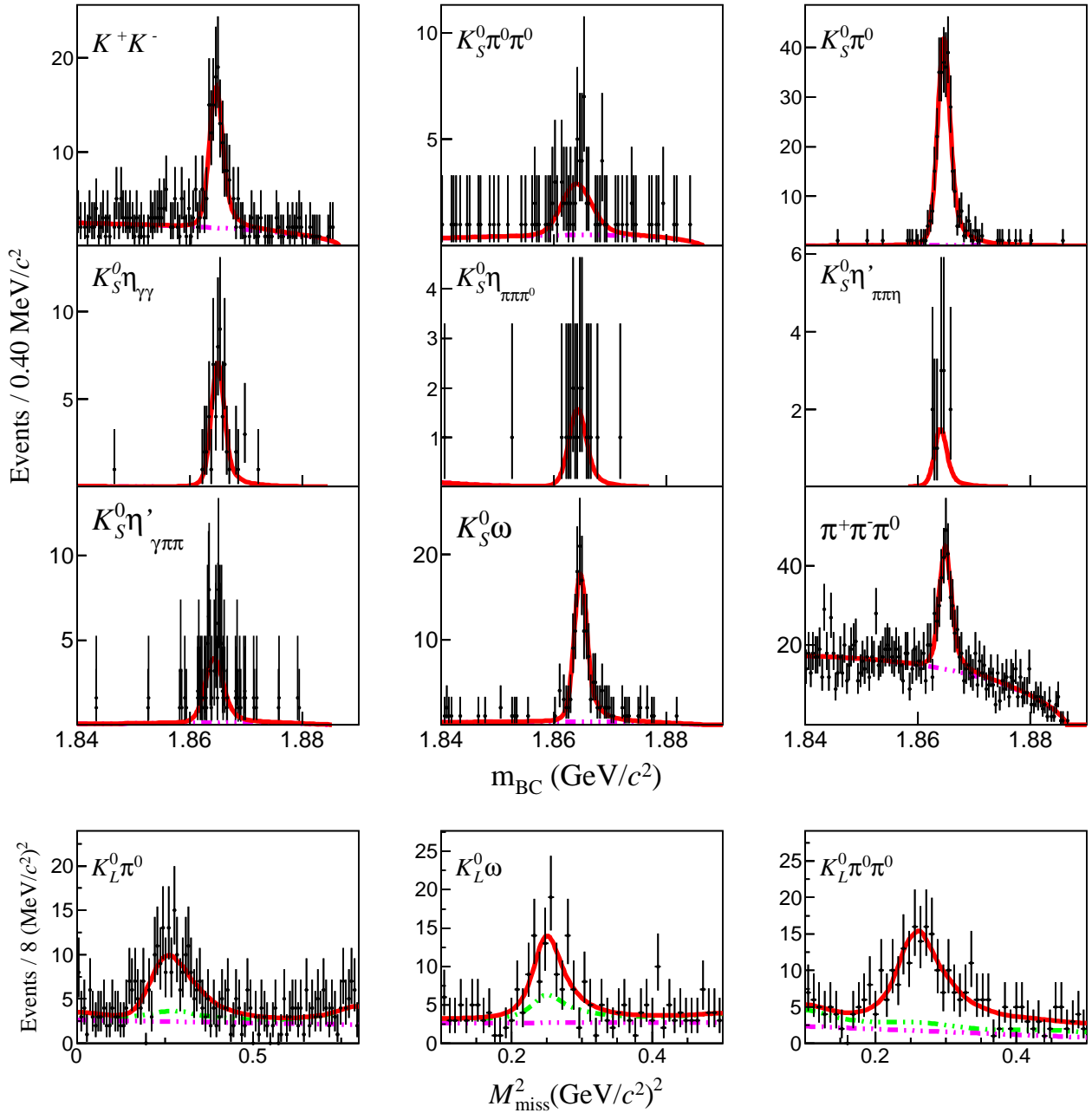


FIG. 2: Distributions and fits used to determine the DT yields. These distributions are of m_{BC} in the fully reconstructed case, and of M_{miss}^2 for the partially reconstructed case involving K_L^0 mesons. In each plot the black dots with error bar are data, the total fit result is shown as the red solid line, the continuum background is shown as the pink dashed line, and sum of the continuum and the peaking background for the $K_L^0 X$ DTs is shown as the green dashed line.

χ^2 per number of degrees of freedom for the N_+ and N_- fits are 6.68/6 and 1.21/3, respectively. It follows from Eq. (3) that

$$F_+^{4\pi} = 0.721 \pm 0.019 \pm 0.007,$$

indicating that the decay $D \rightarrow \pi^+ \pi^- \pi^+ \pi^-$ is predominantly CP -even.

B. $D \rightarrow \pi^+ \pi^- \pi^0$ tag

A second determination of $F_+^{4\pi}$ is made using the quasi CP -even eigenstate $D \rightarrow \pi^+ \pi^- \pi^0$. From the ST and DT yields it follows that

$$N^{\pi\pi\pi^0} = (1.64 \pm 0.21 \pm 0.06) \times 10^{-3},$$

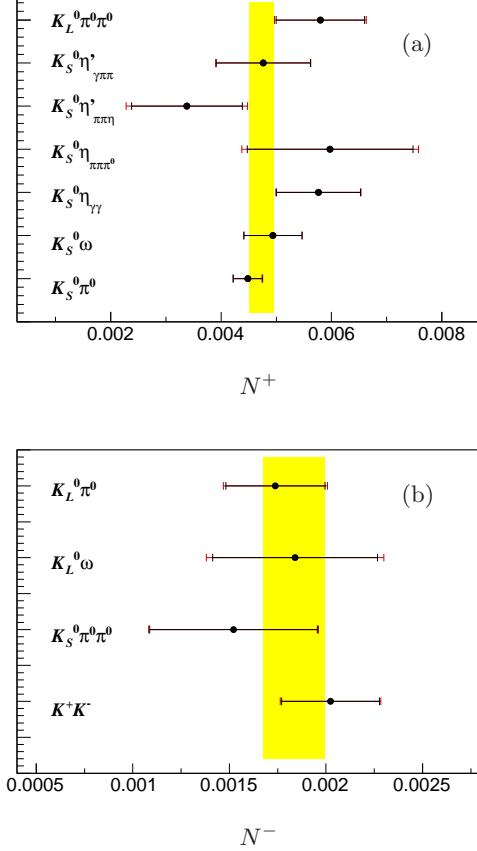


FIG. 3: The results for N^+ (a) and N^- (b). The wide red error bars show the total uncertainties, and the inner black error bars the statistical uncertainties. The yellow bands correspond to the one- σ regions around the mean values.

which, as expected, lies very close to the result for $\langle N^- \rangle$. Using Eq. (6) and the measured value of $F_+^{\pi\pi\pi^0}$ [8] it is found that

$$F_+^{4\pi} = 0.753 \pm 0.028 \pm 0.010,$$

together with a correlation coefficient of 0.15 with the measurement performed with the CP -eigenstate tags, mainly arising from the common use of $\langle N^+ \rangle$ in the two determinations.

C. $D \rightarrow K_{S,L}^0 \pi^+ \pi^-$ tags

The DT events tagged with $D \rightarrow K_{S,L}^0 \pi^+ \pi^-$ decays are analyzed in phase-space bins of the tag channel. The Dalitz plots of these decays have axes corresponding to the squared invariant masses $m_-^2 = m(K_{S,L}^0 \pi^-)^2$ and $m_+^2 = m(K_{S,L}^0 \pi^+)^2$. Eight pairs of bins are defined symmetrically about the line $m_-^2 = m_+^2$ with a positive bin number in the region $m_+^2 > m_-^2$ and a negative one on

the other side of the the line of equality. Bin boundaries have been defined according to the “equal $\Delta\delta_D$ scheme” of Ref. [20], such that the strong-phase difference between symmetric points in the Dalitz plot spans an equal range in each bin, according to the expectations of an amplitude model [35]. For $D \rightarrow K_S^0 \pi^+ \pi^-$, both the CLEO and BESIII collaborations have made measurements of c_i , the cosine of the average strong-phase difference weighted by the D^0 decay amplitude in each bin, and c'_i , the analogous quantity for $D \rightarrow K_L^0 \pi^+ \pi^-$ decays [14, 15, 20]. The current analysis uses the averaged BESIII and CLEO results for c_i and c'_i , together with the BESIII results for K_i and K'_i , which are the probabilities of the D^0 decay occurring in bin i . All of these inputs are reported in Ref. [15].

As is clear from Eq. (7), the expected yields $M_i^{(\prime)}$ are symmetric under the exchange $i \leftrightarrow -i$ and so the yields in these pairs of bins are aggregated in the analysis, giving eight effective bins, labeled 1 through to 8, for each tag mode. The DT yields are determined from independent fits to the events in each effective bin following the procedure already described in Sec. IV. In some regions, the sample sizes are low and it is necessary to fix the parameters of the convolving Gaussian function to those determined from a fit to the whole of phase space. The fitted yields include contamination from peaking background, which is estimated from MC simulation to be at the level of 2.3% and 9.5% for $D \rightarrow K_S^0 \pi^+ \pi^-$ and $D \rightarrow K_L^0 \pi^+ \pi^-$, respectively.

To improve the resolution of the location of the decay in the Dalitz plot, and thereby ensure the most reliable assignment of the phase-space bin, the tag decay is refitted with the D mass constrained to the known mass of the D^0 meson [27]. Even with this constraint in place, there are occasional bin misassignments. These misassignments, and the variations in relative efficiency between bins, are accounted for by an 8×8 efficiency matrix ϵ_{ij} , which is determined from MC simulation:

$$\epsilon_{ij} = \frac{N_{ij}^{\text{rec}}}{N_i^{\text{gen}}}, \quad (9)$$

where N_{ij}^{rec} is the number of signal MC events generated in the i -th bin and reconstructed in the j -th bin, and N_i^{gen} is the number of the signal MC events generated in the i -th bin. The probability of misassignment varies from 5% to 20% depending on the bin and tag channel. The relative variation in efficiency between bins is within 20%. Separate efficiency matrices $\epsilon_{ij}^{K_S^0 \pi \pi}$ and $\epsilon_{ij}^{K_L^0 \pi \pi}$ are determined for each tag mode. The full efficiency matrices can be found in the Appendix.

The efficiency matrices are used to adjust the idealized expressions of Eq. (7), giving expected DT signal yields

in bin i of

$$\begin{aligned}
M_i(4\pi, K_S^0\pi^+\pi^-) &= \\
H \sum_j^8 \epsilon_{ij}^{K_S^0\pi\pi} [K_j + K_{-j} - 2\sqrt{K_j K_{-j}} c_j (2F_+^{4\pi} - 1)], \\
M_i'(4\pi, K_L^0\pi^+\pi^-) &= \\
H' \sum_j^8 \epsilon_{ij}^{K_L^0\pi\pi} [K'_j + K'_{-j} + 2\sqrt{K'_j K'_{-j}} c'_j (2F_+^{4\pi} - 1)].
\end{aligned} \tag{10}$$

The CP -even fraction is then determined by minimizing the negative log-likelihood

$$\begin{aligned}
-2 \log \mathcal{L} &= -2 \log G(M_i^{\text{obs}}; M_i^{\text{exp}}, \sigma_{M_i}) \\
&\quad - 2 \log G(M_i'^{\text{obs}}; M_i'^{\text{exp}}, \sigma_{M_i'}),
\end{aligned} \tag{11}$$

where G is a Gaussian function, $M_i^{(\prime)\text{obs}}$ and $M_i^{(\prime)\text{exp}}$ are the observed and predicted DT yields in bin i , respectively (here including peaking background contributions), and $\sigma_{M_i^{(\prime)}}$ is the uncertainty on $M_i^{(\prime)\text{obs}}$. This fit yields

$$F_+^{4\pi} = 0.754 \pm 0.031 \pm 0.009.$$

Separate fits to the $D \rightarrow K_S^0\pi^+\pi^-$ and $D \rightarrow K_L^0\pi^+\pi^-$ samples give the results 0.813 ± 0.045 and 0.712 ± 0.038 , respectively, with purely statistical uncertainties. These fits are shown in Fig. 4.

D. Assignment of systematic uncertainties

There are several sources of potential systematic bias on the three determinations of $F_+^{4\pi}$, some of which are correlated between two or all of the measurements. The assigned uncertainties are summarized in Table III and are discussed below.

There are systematic uncertainties on N_{ST} and N_{DT} for each tag mode that lead to corresponding uncertainties in the values of $\langle N^+ \rangle$, $\langle N^- \rangle$, and $N^{\pi\pi\pi^0}$. There are various components contributing to these uncertainties. To assess any bias associated with the fit procedure, alternative fits are performed to the m_{BC} distributions for the ST samples and fully reconstructed DT samples, with variations of ± 0.5 MeV applied to the end point of the ARGUS function. The contributions of the peaking backgrounds in all samples are varied according to the uncertainties of their branching fractions [27]. The variation in results is taken as the uncertainty associated with these sources. The effective ST yields for the $D \rightarrow K_L^0 X$ tags have a small uncertainty associated with the total size of the charm-meson sample [33]. The uncertainties arising from the knowledge of the $D \rightarrow K_L^0 X$ branching fractions are also small, as those contributions

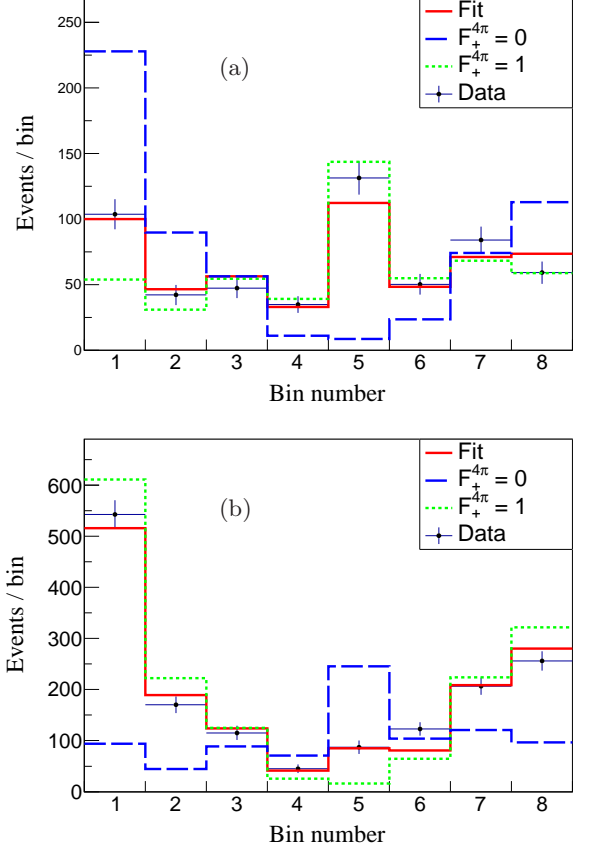


FIG. 4: Fit results for $D \rightarrow K_S^0\pi^+\pi^-$ (a) and $D \rightarrow K_L^0\pi^+\pi^-$ (b) channels. Also shown are the expected distributions in the limiting cases $F_+^{4\pi} = 0$ and $F_+^{4\pi} = 1$.

TABLE III: Summary of systematic contributions for the $F_+^{4\pi}$ measurement performed with CP eigenstate, $D \rightarrow \pi^+\pi^-\pi^0$ and $D \rightarrow K_{S,L}^0\pi^+\pi^-$ tags. The entry ‘/’ indicates that there is no possible bias from the listed source.

Source	CP	$\pi^+\pi^-\pi^0$	$K_{S,L}^0\pi^+\pi^-$
ST and DT yields	0.005	0.003	/
Efficiency factorization	0.003	0.006	/
$F_+^{\pi\pi\pi^0}$	/	0.007	/
$K_i^{(\prime)}$	/	/	0.005
$c_i^{(\prime)}$	/	/	0.004
Bin misassignment	/	/	0.003
$K_{S,L}^0\pi^+\pi^-$ backgrounds	/	/	0.003
K_S^0 veto	0.003	0.003	0.003
Total	0.007	0.010	0.009

to these uncertainties associated with the reconstruction efficiencies [34] are common to the $\epsilon'_{\text{ST}}(K_L^0 X)$ efficiencies in Eq. 8, and so cancel in the measurement of the effective ST yields. The determinations of N^{ST} and N^{DT} are the dominant source of systematic uncertainty for the CP eigenstate tags. The common use of $\langle N^- \rangle$ means that this uncertainty is correlated between the CP -eigenstate measurement and that made with $D \rightarrow \pi^+ \pi^- \pi^0$ tags.

The measurements performed with the CP -eigenstate and the $D \rightarrow \pi^+ \pi^- \pi^0$ tags assume that the DT-event efficiency can be factorized into the reconstruction efficiencies of the two decay modes in a universal manner for all tags. Studies with MC simulation show that this is not exactly true, and so small correction factors obtained from the simulation are applied to each class of DT in the measurement. Shifts of 0.06×10^{-3} and 0.01×10^{-3} are observed in the values of $\langle N^+ \rangle$ and $\langle N^- \rangle$, respectively, and of 0.05×10^{-3} for $N^{\pi\pi\pi^0}$, which are assigned as systematic uncertainties that when propagated to $F_+^{4\pi}$ give the uncertainties listed in Table III.

The quasi- CP -eigenstate measurement carries an uncertainty from the imperfect knowledge of the CP -even fraction of $D \rightarrow \pi^+ \pi^- \pi^0$ [8]. This is the dominant systematic uncertainty for the determination of $F_+^{4\pi}$ using this tag channel.

The measurement performed with $D \rightarrow K_{S,L}^0 \pi^+ \pi^-$ tags has uncertainties associated with the knowledge of the external parameters $K_i^{(\prime)}$ and $c_i^{(\prime)}$. To evaluate the size of these contributions, the measurement is re-performed 1000 times for each set of inputs with the values of the parameters smeared in a manner that corresponds to the covariance matrices reported in Ref. [15]. The spread on the resulting distribution for $F_+^{4\pi}$ over the ensemble of measurements is assigned as the uncertainty of the result from these sources. The efficiency matrix, used to describe bin misassignment and relative bin-to-bin efficiencies, has uncertainties arising from the finite size of the MC sample from which its elements are determined. The effect of these uncertainties, which are most important for bin misassignments, are determined by re-performing the fit 1000 times with smeared inputs. The branching fractions of the peaking backgrounds in these samples are varied within their measured uncertainties to determine the size of the potential bias from this source [27].

A final uncertainty is assigned, common to all three measurements, to account for the possibility that the K_S^0 veto in the DT selection leads to a sample with a different CP -even fraction to that of the unbiased decay. The size of the effect is estimated to be 3×10^{-3} and is determined from the amplitude model by computing $F_+^{4\pi}$ with and without the relevant region of phase space included.

E. Combination of results

The results of the three separate measurements of $F_+^{4\pi}$ are summarized in Table IV. It can be seen that these results are consistent with each other. A combination is made of these measurements, taking account of the correlation coefficient of 0.15 between the CP -eigenstate and $D \rightarrow \pi^+ \pi^- \pi^0$ tags, that yields the result presented in Table IV. This result is consistent with the CLEO-c result of 0.737 ± 0.028 from a measurement that employs a similar analysis strategy and is around twice as precise [8]. It is also compatible with a CLEO-c determination that is based on localized measurements in phase space and has around a 30% smaller uncertainty [9].

TABLE IV: Summary of $F_+^{4\pi}$ results from the different tag channels and the combination of these results, where the first uncertainty is statistical and the second is systematic.

Tag modes	$F_+^{4\pi}$
CP eigenstates	$0.721 \pm 0.019 \pm 0.007$
$D \rightarrow \pi^+ \pi^- \pi^0$	$0.753 \pm 0.028 \pm 0.010$
$D \rightarrow K_{S,L}^0 \pi^+ \pi^-$	$0.754 \pm 0.031 \pm 0.009$
Combination	$0.735 \pm 0.015 \pm 0.005$

VI. SUMMARY

In summary, a measurement has been made of $F_+^{4\pi}$, the CP -even fraction of the decay $D^0 \rightarrow \pi^+ \pi^- \pi^+ \pi^-$, using 2.93 fb^{-1} of $e^+ e^- \rightarrow \psi(3770) \rightarrow D\bar{D}$ data collected by the BESIII experiment. The measurement is the combination of three separate, but consistent, determinations of this parameter made with CP -eigenstate tags, the quasi- CP -eigenstate tag $D \rightarrow \pi^+ \pi^- \pi^0$ and a study of the distributions in phase space of $D \rightarrow K_{S,L}^0 \pi^+ \pi^-$ tags. The CP -even fraction is determined to be

$$F_+^{4\pi} = 0.735 \pm 0.015 \pm 0.005,$$

where the first uncertainty is statistical and the second is systematic. This result is compatible with previous measurements [8, 9], but has a higher precision, and provides valuable input to measurements of the CKM angle γ and charm-mixing studies performed at LHCb and Belle II.

The data set can be further exploited to study the CP content and related parameters in localized regions of phase space, as was demonstrated in Ref. [9]. Such measurements, and improved determinations of $F_+^{4\pi}$, will be particularly interesting with the substantially larger samples that will be collected at BESIII over the coming years [23].

ACKNOWLEDGMENTS

The BESIII collaboration thanks the staff of BEPCII and the IHEP computing center and the supercomputing center of USTC for their strong support. This work is supported in part by National Key R&D Program of China under Contracts Nos. 2020YFA0406400, 2020YFA0406300; National Natural Science Foundation of China (NSFC) under Contracts Nos. 11335008, 11625523, 11635010, 11735014, 11835012, 11935015, 11935016, 11935018, 11961141012, 12022510, 12025502, 12035009, 12035013, 12192260, 12192261, 12192262, 12192263, 12192264, 12192265, 11705192, 11950410506, 12061131003, 12105276, 12122509; the Chinese Academy of Sciences (CAS) Large-Scale Scientific Facility Program; Joint Large-Scale Scientific Facility Funds of the NSFC and CAS under Contract No. U1732263, U1832207, U1832103, U2032111; CAS Key Research Program of Frontier Sciences under Contract No. QYZDJ-SSW-SLH040; 100 Talents Program of CAS; INPAC and Shanghai Key Laboratory for Particle Physics and Cosmology; ERC under Contract No. 758462; European Union's Horizon 2020 research and innovation programme under Marie Skłodowska-Curie grant agreement under Contract No. 894790; German Research Foun-

ation DFG under Contracts Nos. 443159800, Collaborative Research Center CRC 1044, GRK 2149; Istituto Nazionale di Fisica Nucleare, Italy; Ministry of Development of Turkey under Contract No. DPT2006K-120470; National Science and Technology fund; National Science Research and Innovation Fund (NSRF) via the Program Management Unit for Human Resources & Institutional Development, Research and Innovation under Contract No. B16F640076; STFC (United Kingdom); Suranaree University of Technology (SUT), Thailand Science Research and Innovation (TSRI), and National Science Research and Innovation Fund (NSRF) under Contract No. 160355; The Royal Society, UK under Contracts Nos. DH140054, DH160214; The Swedish Research Council; U. S. Department of Energy under Contract No. DE-FG02-05ER41374.

APPENDIX: EFFICIENCY MATRICES

The efficiency matrices for $\pi^+\pi^-\pi^+\pi^-$ vs. $K_{S,L}^0\pi^+\pi^-$ giving the efficiency in each bin and migration probabilities between bins are shown in Table V.

-
- [1] M. Gronau and D. London, *How to determine all the angles of the unitarity triangle from $B_d^0 \rightarrow DK_S$ and $B_s^0 \rightarrow D\phi$* , *Phys. Lett. B* **253** (1991) 483.
- [2] M. Gronau and D. Wyler, *On determining a weak phase from CP asymmetries in charged B decays*, *Phys. Lett. B* **265** (1991) 172.
- [3] A. Lenz and G. Wilkinson, *Mixing and CP Violation in the Charm System*, *Ann. Rev. Nucl. Part. Sci.* **71** (2021) 59 [[arXiv:2011.04443](#)].
- [4] M. Nayak, J. Libby, S. Malde, C. Thomas, G. Wilkinson, R. A. Briere et al., *First determination of the CP content of $D \rightarrow \pi^+\pi^-\pi^0$ and $D \rightarrow K^+K^-\pi^0$* , *Phys. Lett. B* **740** (2015) 1 [[arXiv:1410.3964](#)].
- [5] S. Malde, C. Thomas and G. Wilkinson, *Measuring CP violation and mixing in charm with inclusive self-conjugate multibody decay modes*, *Phys. Rev. D* **91** (2015) 094032 [[arXiv:1502.04560](#)].
- [6] BaBar Collaboration, *Evidence for direct CP violation in the measurement of the Cabibbo-Kobayashi-Maskawa angle γ with $B^\mp \rightarrow D^{(*)}K^{(*)\mp}$ decays*, *Phys. Rev. Lett.* **105** (2010) 121801 [[arXiv:1005.1096](#)].
- [7] Belle Collaboration, *Evidence for direct CP violation in the decay $B \rightarrow D^{(*)}K$, $D \rightarrow K_S^0\pi^+\pi^-$ and measurement of the CKM phase ϕ_3* , *Phys. Rev. D* **81** (2010) 112002 [[arXiv:1003.3360](#)].
- [8] S. Malde, C. Thomas, G. Wilkinson, P. Naik, C. Prouve, J. Rademacker et al., *First determination of the CP content of $D \rightarrow \pi^+\pi^-\pi^+\pi^-$ and updated determination of the CP contents of $D \rightarrow \pi^+\pi^-\pi^0$ and $D \rightarrow K^+K^-\pi^0$* , *Phys. Lett. B* **747** (2015) 9 [[arXiv:1504.05878](#)].
- [9] S. Harnew, P. Naik, C. Prouve, J. Rademacker and D. Asner, *Model-independent determination of the strong phase difference between D^0 and $\bar{D}^0 \rightarrow \pi^+\pi^-\pi^+\pi^-$ amplitudes*, *JHEP* **01** (2018) 144 [[arXiv:1709.03467](#)].
- [10] P. K. Resmi, J. Libby, S. Malde and G. Wilkinson, *Quantum-correlated measurements of $D \rightarrow K_S^0\pi^+\pi^-\pi^0$ decays and consequences for the determination of the CKM angle γ* , *JHEP* **01** (2018) 082 [[arXiv:1710.10086](#)].
- [11] LHCb Collaboration, *Measurement of CP observables in $B^\pm \rightarrow DK^\pm$ and $B^\pm \rightarrow D\pi^\pm$ with two- and four-body D decays*, *Phys. Lett. B* **760** (2016) 117 [[arXiv:1603.08993](#)].
- [12] LHCb Collaboration, *Measurement of CP observables in the process $B^0 \rightarrow DK^{*0}$ with two- and four-body D decays*, *JHEP* **08** (2019) 041 [[arXiv:1906.08297](#)].
- [13] BESIII Collaboration, *Measurement of the $D \rightarrow K^-\pi^+$ strong phase difference in $\psi(3770) \rightarrow D^0\bar{D}^0$* , *Phys. Lett. B* **734** (2014) 227 [[arXiv:1404.4691](#)].
- [14] BESIII Collaboration, *Determination of strong-phase parameters in $D \rightarrow K_{S,L}^0\pi^+\pi^-$* , *Phys. Rev. Lett.* **124** (2020) 241802 [[arXiv:2002.12791](#)].
- [15] BESIII Collaboration, *Model-independent determination of the relative strong-phase difference between D^0 and $\bar{D}^0 \rightarrow K_{S,L}^0\pi^+\pi^-$ and its impact on the measurement of the CKM angle γ/ϕ_3* , *Phys. Rev. D* **101** (2020) 112002 [[arXiv:2003.00091](#)].
- [16] BESIII Collaboration, *Improved model-independent*

- determination of the strong-phase difference between D^0 and $\bar{D}^0 \rightarrow K_{S,L}^0 K^+ K^-$ decays, *Phys. Rev. D* **102** (2020) 052008 [arXiv:2007.07959].
- [17] BESIII Collaboration, Measurement of the $D \rightarrow K^- \pi^+ \pi^+ \pi^-$ and $D \rightarrow K^- \pi^+ \pi^0$ coherence factors and average strong-phase differences in quantum-correlated $D\bar{D}$ decays, *JHEP* **05** (2021) 164 [arXiv:2103.05988].
- [18] HFLAV Collaboration, Averages of b -hadron, c -hadron, and τ -lepton properties as of 2018, arXiv:1909.12524, December 2021 update (updated results and plots available at <https://hflav.web.cern.ch/>).
- [19] T. Gershon, J. Libby and G. Wilkinson, Contributions to the width difference in the neutral D system from hadronic decays, *Phys. Lett. B* **750** (2015) 338 [arXiv:1506.08594].
- [20] CLEO Collaboration, Model-independent determination of the strong-phase difference between D^0 and $\bar{D}^0 \rightarrow K_{S,L}^0 h^+ h^-$ ($h = \pi, K$) and its impact on the measurement of the CKM angle γ/ϕ_3 , *Phys. Rev. D* **82** (2010) 112006 [arXiv:1010.2817].
- [21] BESIII Collaboration, Design and construction of the BESIII detector, *Nucl. Instrum. Meth. A* **614** (2010) 345 [arXiv:0911.4960].
- [22] C. Yu et al., BEPCII performance and beam dynamics studies on luminosity, in 7th International Particle Accelerator Conference, 2016, DOI.
- [23] BESIII Collaboration, Future physics programme of BESIII, *Chin. Phys. C* **44** (2020) 040001 [arXiv:1912.05983].
- [24] GEANT4 Collaboration, GEANT4 – a simulation toolkit, *Nucl. Instrum. Meth. A* **506** (2003) 250.
- [25] S. Jadach, B. Ward and Z. Was, The precision Monte Carlo event generator KK for two fermion final states in e^+e^- collisions, *Comput. Phys. Commun.* **130** (2000) 260 [hep-ph/9912214].
- [26] D. Lange, The EvtGen particle decay simulation package, *Nucl. Instrum. Meth. A* **462** (2001) 152.
- [27] Particle Data Group, Review of particle physics, *PTEP* **2020** (2020) 083C01.
- [28] J. C. Chen, G. S. Huang, X. R. Qi, D. H. Zhang and Y. S. Zhu, Event generator for J/ψ and $\psi(2S)$ decay, *Phys. Rev. D* **62** (2000) 034003.
- [29] Y. Rui-Ling, P. Rong-Gang and C. Hong, Tuning and validation of the Lundcharm model with J/ψ decays, *Chin. Phys. Lett.* **31** (2014) 061301.
- [30] E. Richter-Was, QED bremsstrahlung in semileptonic B and leptonic τ decays, *Phys. Lett. B* **303** (1993) 163 .
- [31] BaBar Collaboration, Measurement of D^0 - \bar{D}^0 mixing parameters using $D^0 \rightarrow K_S^0 \pi^+ \pi^-$ and $D^0 \rightarrow K_S^0 K^+ K^-$ decays, *Phys. Rev. Lett.* **105** (2010) 081803 [arXiv:1004.5053].
- [32] ARGUS Collaboration, Search for hadronic $b \rightarrow u$ decays, *Phys. Lett. B* **241** (1990) 278 .
- [33] BESIII Collaboration, Measurement of $e^+e^- \rightarrow D\bar{D}$ cross sections at the $\psi(3770)$ resonance, *Chin. Phys. C* **42** (2018) 083001 [arXiv:1803.06293].
- [34] BESIII Collaboration, Improved measurement of the strong-phase difference $\delta_D^{K\pi}$ in quantum-correlated $D\bar{D}$ decays, arXiv:2208.09402.
- [35] BaBar Collaboration, Improved measurement of the CKM angle γ in $B^\mp \rightarrow D^{(*)} K^{(*)\mp}$ decays with a Dalitz plot analysis of D decays to $K_S^0 \pi^+ \pi^-$ and $K_S^0 K^+ K^-$, *Phys. Rev. D* **78** (2008) 034023 [arXiv:0804.2089].

TABLE V: Efficiency matrix ϵ_{ij} (%) for $\pi^+\pi^-\pi^+\pi^-$ vs. $K_{S,L}^0\pi^+\pi^-$. The column gives the true bin i , while the row gives the reconstructed bin j .

Bins	1	2	3	4	5	6	7	8
ϵ_{ij} for $\pi^+\pi^-\pi^+\pi^-$ vs. $K_S^0\pi^+\pi^-$								
1	0.2928	0.0103	0.0014	0.0005	0.0012	0.0009	0.0013	0.0139
2	0.0219	0.2965	0.0121	0.0003	0.0012	0.0006	0.0015	0.0026
3	0.0029	0.0089	0.3424	0.0062	0.0023	0.0010	0.0008	0.0009
4	0.0015	0.0005	0.0110	0.3394	0.0080	0.0015	0.0008	0.0011
5	0.0020	0.0004	0.0011	0.0035	0.3070	0.0074	0.0010	0.0013
6	0.0023	0.0005	0.0013	0.0008	0.0156	0.2810	0.0176	0.0020
7	0.0028	0.0010	0.0009	0.0006	0.0016	0.0134	0.2698	0.0186
8	0.0252	0.0019	0.0010	0.0004	0.0010	0.0012	0.0188	0.2701
ϵ_{ij} for $\pi^+\pi^-\pi^+\pi^-$ vs. $K_L^0\pi^+\pi^-$								
1	0.4216	0.0167	0.0010	0.0002	0.0005	0.0008	0.0028	0.0276
2	0.0399	0.4139	0.0150	0.0005	0.0008	0.0012	0.0024	0.0046
3	0.0026	0.0177	0.4366	0.0073	0.0018	0.0009	0.0030	0.0023
4	0.0015	0.0026	0.0196	0.4497	0.0107	0.0026	0.0030	0.0007
5	0.0002	0.0003	0.0009	0.0060	0.4164	0.0150	0.0016	0.0009
6	0.0039	0.0015	0.0011	0.0013	0.0174	0.3653	0.0371	0.0045
7	0.0071	0.0016	0.0006	0.0004	0.0010	0.0164	0.3753	0.0415
8	0.0476	0.0039	0.0006	0.0001	0.0005	0.0013	0.0364	0.3683